Published in final edited form as:
Neurochem Int. 2008 June ; 52(7): 1365–1372.

Electrophysiological properties and gap junction coupling of striatal astrocytes

Adermark Louise and **David M Lovinger***
Section on Synaptic Pharmacology, Laboratory for Integrative Neuroscience, NIAAA/NIH, Bethesda, Maryland 20892

Abstract

The striatum is the biggest nucleus of the basal ganglia and receives input from almost all cortical regions, substantia nigra and the thalamus. Striatal neuronal circuitry is well characterized, but less is known about glial physiology. To this end, we evaluated astrocyte electrophysiological properties using whole-cell patch-clamp recording in dorsal striatal brain slices from P15 – P21 rat. The majority of cells (95%) were passive astrocytes that do not express any detectable voltage-gated channels. Passive astrocytes were subcategorized into three groups based on time dependent current properties. The observed proportion of the different astrocyte subtypes did not change within the age range evaluated here, but was modulated during reduction of specific conductances and gap junction coupling. Striatal astrocytes were extensively interconnected and closure of gap junctions with octanol (1 mM), carbenoxolone (100 μM) or increased intracellular calcium (2 mM), significantly altered intrinsic properties. When simultaneously blocking potassium channels and gap junction coupling almost no passive conductance was detected, implying that the major currents in striatal astrocytes derive from potassium and gap junction conductance. Uncoupling of the syncytium reduced currents activated in response to a hyperpolarizing pulse, suggesting that changes in gap junction coupling alters astrocyte electrophysiological responses. Our findings indicate that the prevalent gap junction coupling is vital for astrocyte function in the striatum, and that whole cell recordings will be distorted by currents activated in neighboring cells.

Keywords

Astroglia; basal ganglia; carbenoxolone; glia; patch clamp

INTRODUCTION

The striatum is the largest component of the basal ganglia and is considered a critical nexus that receives glutamatergic input from almost all parts of the cortex and the thalamus (Tepper et al., 2007). The striatum regulates the chain of neuronal responses leading to motor acts and plays an important role in instrumental learning (Balleine et al., 2007; Graybiel et al., 1994). Although much is known about the circuitry and neuronal physiology of striatum, the electrophysiological properties of striatal glial cells have not been well characterized. Astrocytes are a subtype of glia cell that have pivotal roles in neuronal development and

Corresponding author: David M. Lovinger, Section on Synaptic Pharmacology, Laboratory for Integrative Neuroscience, NIAAA/NIH, 5625 Fishers Lane, TS-13, Bethesda, Maryland 20892, Telephone: 001-301-443-2445, Fax: 001-301-480-0466, e-mail: lovindav@mail.nih.gov.

function (Freeman, 2006; Ransom et al., 2003; Slezak and Pfrieger, 2003). Astrocyte clearance of neuroactive substances from the synaptic cleft is well established (Simard and Nedergaard, 2004; Waagepetersen et al., 2005), and astrocyte/neuronal communication involving diverse receptor systems has also been described (Nedergaard et al., 2003; Schipke and Kettenmann, 2004). Furthermore, astrocytes form a syncytium as they are interconnected through gap junction channels, formed by the protein connexin (Dermietzel et al., 1991; Dermietzel and Spray, 1993). Gap junction channels connect the cytoplasm of adjacent cells, and are crucial for synchronization of astrocytic signaling, calcium wave propagation, and spatial buffering of potassium (Blomstrand et al., 1999a; Cotrina et al., 1998; Giaume and Venance, 1998; Wallraff et al., 2006). Astrocyte gap junction coupling can be modulated by various neuroactive substances, suggesting that channels open and close in response to neuronal activity (Blomstrand et al., 1999b; Blomstrand et al., 2004; Enkvist and McCarthy, 1994; Rouach et al., 2000; Venance et al., 1995).

Studies from other brain regions and cell cultures have shown that astrocytes are pharmacologically and functionally heterogeneous, and that different subtypes of astrocytes are electrophysiologically distinct (Davis-Cox et al., 1994; Venance et al., 1998; Wallraff et al., 2004; Zhou et al., 2006). The aim of this study was to evaluate electrophysiolgical properties and gap junction coupling of astrocytes in the dorsal striatum. Immunohistochemical staining of striatal brain slices has shown that astrocytes reach a final population at P21 (Domaradzka-Pytel et al., 2000) therefore we used brain slices from P15–21-day-old Sprague Dawley rats to evaluate astrocyte properties during this developmental period. Our data show that the majority of astrocytes in the striatum are passive cells that are extensively interconnected through gap junction channels.

EXPERIMENTAL PROCEDURES

Preparation of brain slices

Striatal slices were prepared from 15–21-day-old Sprague Dawley rats as previously described (Adermark and Lovinger, 2006). In brief, animals were deeply anesthetized in halothane and decapitated. The brains were placed in ice-cold modified artificial cerebrospinal fluid (aCSF) containing (in mM); 194 sucrose, 30 NaCl, 4.5 KCl, 1 $MgCl_2$, 26 $NaHCO_3$, 1.2 NaH_2PO_4 and 10 D-glucose, and cut into 350 μm thick coronal slices containing the striatum and cortex. Brain slices were allowed to equilibrate for at least 1 h at room temperature in normal aCSF containing (in mM); 124 NaCl, 4.5 KCl, 2 $CaCl_2$, 1 $MgCl_2$, 26 $NaHCO_3$, 1.2 NaH_2PO_4 and 10 D-glucose continuously bubbled with a mixture of 95% O_2/5% CO_2 gas.

Electrophysiology

Electrophysiological recordings were performed as previously described (Adermark and Lovinger, 2006). Currents were measured in conventional ruptured-patch whole-cell mode using pipettes with a typical resistance of 2–6 MΩ when filled with internal solution containing (in mM); KCl 130, $MgCl_2$ 2, HEPES 10, EGTA 5, Na-ATP 2, $CaCl_2$ 0.5, with pH set to 7.3 with KOH unless otherwise stated. In some recordings gap junction coupling was blocked by increasing intracellular calcium ($[Ca^{2+}]_i$) to 2 mM with $CaCl_2$ (Enkvist and McCarthy, 1994). Other internal solutions used contained CsCl as a substitute for KCl, a combination of CsCl substitution and elevated internal calcium, or 10 mM BAPTA as a substitute for EGTA and $CaCl_2$. We also used a $CsMeSO_3$-based internal solution containing (in mM); 120 $CsMeSO_3$, 5 NaCl, 10 TEA-Cl, 10 Hepes, 5 QX-314, 1.1 EGTA, 4 Mg-ATP, 0.3 Na-GTP, with pH set at 7.2 with CsOH. Intracellular solutions were filtered, and osmolarities of intracellular solutions and aCSF were set with sucrose to 300 mmol/kg and 314 mmol/kg, respectively.

Input resistance was calculated by measuring current in response to a 5 mV pulse with 10 ms duration. Resting membrane potential was determined by finding the membrane potential at which the steady-state current level was zero (0 current level), and apparent capacitance was measured from capacitive transients generated by the 5 mV pulse. To minimize the influence of the internal solution on initial estimates of intrinsic properties, measurements were taken immediately after establishing whole-cell configuration. During prolonged recordings intrinsic properties were monitored continuously and data collected after 15 min. Current-voltage (I/V) relationships were measured to determine the presence or absence of voltage-gated currents. The membrane potential was stepped for 250 ms from the holding potential of −70 mV to hyper- and depolarizing potentials ranging from −130 to 60 mV, in 10 mV increments. A leak subtraction algorithm that was based on the input resistance of individual cells was employed to the I/V relationships in order to more clearly detect voltage-gated currents in these cells. Presented data are raw-data. The response to weak hyperpolarization was evaluated by subjecting cells to 150 ms pulses of −20 mV from the holding potential of −70 mV delivered 1/10 sec.

All drugs were purchased from Sigma (St Louis, MO). 4-aminopyridine (4-AP) was dissolved in aCSF, octanol was dissolved in DMSO to 3.1% and diluted in aCSF to a final concentration of 1 mM, while carbenoxolone (Cbx) was dissolved in water (150 mM) and diluted in aCSF to a final concentration of 100 μM. Drugs and aCSF was applied through the gravity-assisted perfusion system. All recordings were performed at 30°C.

Immunohistochemistry and dye filling

For evaluation of the degree of gap junction coupling, one astrocyte was loaded with the low molecular weight dye Lucifer Yellow (0.05 mg/ml) (Sigma). Brain slices were perfused with aCSF, octanol or Cbx, in the recording chamber for 15 min before whole the cell configuration was established, and patch clamped cells were held at −70 mV for 10 min during which time the dye was allowed to spread throughout the syncytium. Slices were fixed overnight in 4% formaldehyde in 0.1 M phosphate buffered saline (PBS) at 4 °C, then washed and kept in PBS at 4 °C. The number of stained cells was calculated by manually counting in-focus cells on 2D images captured with an Axiovert 200 epiflourescence microscope using a 10x, N.A 0.30, Plan-NEOFLUAR objective and an AxioCam MR monochrome camera (Carl Zeiss Inc., Thornwood, NY).

For morphological evaluation post recording, a subset of patch clamped cells were filled via the patch pipette with Lucifer Yellow and/or Texas Red (5 mg/ ml) (Molecular probes, Invitrogen Corporation, Carlsbad, CA) as previously described (Adermark and Lovinger, 2006). In brief, after fixation, brain slices were delipidated using an ethanol gradient (70, 80, 95, 100, 95, 80, 70 %) before incubating in PBS containing 0.2% Triton X 100 (PBS-T) for 2 hours, followed by 5% BSA in PBS-T overnight. To identify astrocytes, neurons and oligodendrocytes, slices were incubated for 48–72 h at 4 °C with antibodies against glial fibrillary acidic protein (GFAP) [mouse monoclonal (1:200)], microtubule associated protein 2 (MAP2) [rabbit polyclonal (1:200)] or olig1 [rabbit polyclonal (1:200)] (Chemicon, Temecula, CA). After rinsing, slices were incubated with secondary antibodies [Alexa 568 anti mouse (1:1000) or Alexa 568 anti rabbit (1:500)] for at least 15 h. Brain slices were washed 3 × 1h in PBS-T, rinsed with TBS, mounted with Prolong antifade medium (Molecular probes, Invitrogen Corporation) in secure-seal™ spacers (Molecular Probes) attached to coverslips (No 1.5; 24×60 mm, Corning, NY, USA) and sealed with coverglass (Corning No. 1) and nail polish, before being viewed with an Axiovert 200 epiflourescence microscope (Carl Zeiss Inc., Thornwood, NY). The filter cubes used for imaging Lucifer Yellow had the following properties; excitation filter D480/30x, Dichroic mirror 505 DCLP with emitted light filtered through a D535/40m. Alexa 568 was excited through a D540/25x filter. The dichroic mirror

was 565 DCLP and emitted light was filtered through a bandpass filter D605/55m. Images were captured using an AxioCam MR monochrome camera (Carl Zeiss Inc.) and AxioVision 3.1 software. Images were assembled in Photoshop.

Statistics

Statistical comparisons between groups of cells were performed by one-way ANOVA with Tukey's Multiple Comparison Test, or when applicable, with paired t-test. For comparison of membrane current pattern we used Fisher's exact test (Graph Pad Software Inc., San Diego, CA). The level of significance is presented in each figure.

RESULTS

Membrane current pattern and electrophysiological properties of striatal astrocytes

Categorization of cells was made based on whole cell patch clamp recordings from over 200 astrocytes in the dorsal striatum. Cells were classified as passive or complex based on the absence (passive) or presence (complex) of voltage-gated currents under our recording conditions. The majority of cells (95%) were passive astrocytes that exhibited relatively linear current/voltage relationships. Three different membrane current patterns could be distinguished in this group of cells, and are referred to as A1, A2 and A3 astrocytes (Fig 1) (Compare to (Anderova et al., 2004)). Cells with an A1 current pattern (56%) exhibited a large voltage independent conductance and a slowly decaying current component. A2 astrocytes (19%) displayed voltage independent currents with a slowly activating component, while A3 astrocytes (20%) only showed time- and voltage independent conductance. The intrinsic properties of the passive cells were similar across groups, but astrocytes with an A3 current pattern displayed a significantly lower capacitance compared to cells with an A2 membrane current pattern (Table I). We did not find evidence of voltage-gated currents after leak subtraction in these cells.

Five percent of the cells examined were categorized as complex astrocytes that expressed a combination of time- and voltage-activated currents (Fig. 1). The majority of these currents were outward, and we did not detect any fast inward currents upon depolarization. Complex astrocytes had a higher input resistance and lower capacitance compared to passive astrocytes (Table I).

P15–P21 development

The proportion of electrophysiologically-defined astrocyte subtypes did not vary across the age range evaluated here (Complex vs. passive astrocytes, P15 vs. P21, Fisher’s exact test, $p > 0.05$) (Fig. 2a). Intrinsic properties were also relatively stable. Resting membrane potential in cells from P21 slices was more positive in comparison to cells at earlier developmental time points (P15 $p < 0.001$, P16 $p < 0.05$; P19 $p < 0.05$), but input resistance and apparent capacitance did not differ significantly within this age span (Fig. 2b).

Electrophysiological properties during prolonged recordings

Astrocytic currents were evaluated by performing manipulations designed to reduce particular cellular conductances. Chelation of intracellular calcium with 10 mM BAPTA had no significant effect on intrinsic membrane properties (Table II), and the decrease in astrocytes with an A3 current pattern was not significant compared to control (KCl-loaded cells, Fisher's exact test: $p > 0.05$) (Fig. 1c, Fig. 3). Potassium channels were blocked by intracellular loading with Cs^+ (CsCl or $CsMeSO_3$) via the patch pipette. CsCl-loaded astrocytes displayed reduced capacitance, the proportion of astrocytes expressing an A3 current pattern increased ($p < 0.05$), and the proportion of A1 expressing astrocytes was significantly reduced ($p < 0.05$). The

intrinsic properties of $CsMeSO_3$-loaded astrocytes were not significantly different compared to control (Table II, Fig. 3). In a subset of experiments we increased $[Ca^{2+}]_i$ in the $CsMeSO_3$-based internal solution to resemble the concentration present in the CsCl-based solution (0.5 mM). In these cells the apparent capacitance was significantly reduced and astrocytes with A3 current pattern increased ($p < 0.05$) (Table II, Fig. 3). In some of the $CsMeSO_3$-loaded astrocytes a transient outward current seemed to be activated, but this finding was not prevalent, and not seen in any of the cells loaded with $CsMeSO_3$-based internal containing $[Ca^{2+}]_i$. No fast inward currents were detected upon depolarization in any astrocyte. Representative traces from BAPTA- and Cs^+-loaded astrocytes are shown in figure 4.

Extracellular application of 4-AP (4 mM) was used as an additional manipulation designed to evaluate the role of potassium conductance. Current was depressed by 4-AP in all experiments. Slope conductance was reduced to 82 % of control value (95% confidence interval 5.2 %; n = 5), and 4 out of 5 cells displayed an A3 current pattern in the presence of 4-AP, which was significantly higher compared to control ($p < 0.05$) (Fig. 5).

In control cells (KCl-loaded) prolonged recordings (>10 min) increased input resistance ($p < 0.01$), but did not affect resting membrane potential or apparent capacitance (Table II). Membrane current pattern was altered compared to baseline in less than 5% of the cells evaluated (2 out of 47 cells), and we did not detect any passive astrocytes that transformed to display a complex configuration. Interestingly, we found that measured capacitance varied extensively (> 30 pF) over the time course of individual recordings, even after the initial stabilization period following establishment of the whole cell configuration (≥5 min). Unstable capacitance that was bidirectional after the first 5 min of stabilization, was detected in 62% of the KCl-loaded astrocytes (29 out of 47) while 46% of the BAPTA-loaded cells were unstable (6 out of 13), suggesting that this variation is not connected to changes in intracellular calcium. Blocking potassium channels with Cs^+, on the other hand, increased the stability. Fluctuating capacitance was detected in 10% (2 out of 20) and 11% (2 out of 18) of the CsCl- and $CsMeSO_3$-loaded cells, respectively. No change in apparent capacitance was seen over time in slices treated with gap junction blockers (see below), suggesting that the change in apparent capacitance might be connected to a dynamic gap junction permeability. Representative time courses of normalized capacitance are shown in Figure 6.

Gap junction coupling in the striatum

To evaluate the degree of gap junction coupling in the striatum we loaded astrocytes with Lucifer Yellow, which has a low molecular weight and easily transfers through gap junction channels (Adermark et al., 2004). Analysis of dye spreading indicated an extensive network of connected astrocytes in the striatum. Lucifer Yellow spread to 510 ± 270 surrounding cells within 10 minutes after establishing whole cell recordings (n = 15 slices), which is similar to data previously reported from this laboratory (Adermark and Lovinger, 2006). In several slices, Lucifer Yellow was detected in cortical astrocytes, further demonstrating the extensive astrocytic network (Fig. 7a). Fifteen min perfusion of octanol (1 mM), or Cbx (100 μM) before establishing the whole cell configuration significantly reduced the number of cells loaded with Lucifer Yellow (82 ± 16, n = 8 (octanol); 127 ± 32, n = 15 (Cbx); octanol vs. Cbx, $p > 0.05$) (Fig. 7b), suggesting that the spreading of Lucifer Yellow is dependent on gap junction coupling.

Electrophysiological properties during blocked gap junction coupling

We employed three different approaches to block gap junction coupling; extracellular octanol (1 mM), extracellular Cbx (100 μM) and increased intracellular $CaCl_2$ (2 mM). All treatments decreased astrocyte conductance, increased input resistance and decreased apparent capacitance to a similar extent, suggesting that these changes are related to decreased

permeability through gap junction channels (Table II; Representative traces are shown in Fig. 4). Blockade of gap junctions with octanol or Cbx shifted resting membrane potential toward more positive values, while $CaCl_2$ had no significant effect on membrane potential (Table II). Even though intrinsic properties resembled values obtained from complex astrocytes, analyzed cells still displayed a passive membrane current pattern. The proportion of A3 astrocyte subtype was significantly increased when gap junctions were blocked by Cbx or increased $[Ca^{2+}]_i$ ($p < 0.01$ (Cbx) and $p < 0.001$ (Ca^{2+})), but not in octanol treated slices (Fig. 3). A mild inward rectification was indicated in some astrocytes during octanol treatment (Fig. 4), but when combing data from all recordings, this rectification was not significantly different from control slices ($p > 0.05$, Anova).

Based on the extensive astrocyte network and the significant changes in intrinsic properties detected during blockade of gap junction channels, electrophysiological properties might be distorted by conductance from connected cells when gap junction channels are fully open. Therefore, in a subset of cells we blocked gap junction- and potassium channels simultaneously through intracellular loading of Ca^{2+} and Cs^{+}. In these cells almost no passive conductance was detected after a 15 min cell loading period, which suggests that the major currents in passive astrocytes derive from potassium and gap junction conductances (Fig. 4d). It also implies that in order to measure conductance deriving from one distinct astrocyte, gap junction channels need to be fully closed.

Impaired astrocyte signaling during blocked gap junction coupling

We then evaluated whether the response to a weak hyperpolarizing pulse (− 20 mV) would be affected by an impaired astrocyte network. After a stable baseline, slices were treated for 15 min with octanol or Cbx. Blocked gap junction coupling reduced the activated response to 52 ± 15% (octanol, n = 5, $p < 0.001$), and 50 ± 8.0% (Cbx, n = 4, $p < 0.001$) (Fig. 8). The same set of experiment could not be performed in cells where gap junction coupling was blocked by intracellular Ca^{2+}-loading, since this did not provide a reliable and stable control state. However, 15 min perfusion of Cbx did not reduce the response to a hyperpolarizing pulse in cells loaded with 2 mM $CaCl_2$, suggesting that increased $[Ca^{2+}]_i$ close gap junction channels and impair astrocyte responses to a similar extent as Cbx treatment (100 ± 1.6% (n = 4, $p > 0.05$) (Fig. 8).

Immunohistochemistry

Immunohistochemistry post recording revealed that patch clamped cells were astrocytes (Fig. 7c). The morphology of GFAP positive and Lucifer Yellow stained astrocytes varied extensively, and the immunoreactivity for GFAP was lower in the striatum than in the overlying white matter (Fig. 7a). As no complex cell was encountered during loading with Lucifer Yellow, we could not make a morphological characterization that could separate passive cells from complex astrocytes. No Lucifer Yellow stained cell was immunopositive for Olig1 or MAP2.

DISCUSSION

Passive astrocytes outnumber complex cells in the striatal slice

Electrophysiological examination of astrocytes in striatal brain slices revealed that the number of passive cells is high, while only a few cells exhibit voltage-gated currents. There is a possibility that these currents are masked by the conductance of the syncytium, but neither leak subtraction, nor blockade of gap junction coupling, provided proofs of any voltage-gated currents in passive astrocytes. The high number of passive cells is in line with a recent study from the nucleus accumbens (D'Ascenzo et al., 2007), while studies from other brain regions have shown a larger population of complex astrocytes (Anderova et al., 2004; Bordey and

Sontheimer, 1998; Isokawa and McKhann, 2005). The difference in proportion is likely dependent on the brain region analyzed and may be connected to the prevalence of gap junction coupling (Sontheimer et al., 1991). However, the number of passive astrocytes have been shown to increase by age in other parts of the CNS, and the difference in proportion of passive and complex cell could therefore be connected to differences in age of the animals used (Chvatal et al., 1995; Zhou et al., 2006). Since the number of complex cells is reduced by age, we do not expect the ratio of passive cells to be significantly altered in striatal slices from older animals.

Intrinsic properties in passive and complex astrocytes

Input resistance was significantly higher and capacitance lower in complex cells, which might reflect a lower degree of gap junction coupling. In line with this hypothesis is a study from mice hippocampus, showing that only one out of two distinct astrocyte subtypes express gap junctions (Wallraff et al., 2004). However, since no complex cell was loaded with Lucifer Yellow, we cannot confirm that complex astrocytes in the striatum are less interconnected.

Importantly, even though membrane potential was measured immediately after establishing the whole cell configuration, the recorded values could still be influenced by the internal solution, and the composition of the extracellular solution.

Electrophysiological properties during prolonged recordings

The distribution of passive astrocyte subtypes (A1–A3) was dependent on intracellular solution and gap junction coupling, suggesting that the membrane current pattern is directly connected to specific conductances in patch clamped cells or related to the degree of gap junction coupling. We did not detect any cell that expressed A3 membrane current pattern in BAPTA loaded cells, while only the A3 subtype was detected in Ca^{2+}-loaded astrocyte, indicating that the level of intracellular calcium modulates the membrane current pattern. However, it is also possible that the chelation of Ca^{2+} enhance the gap junction coupling, and current activated in surrounding cells distort the membrane current pattern in BAPTA loaded cells.

By blocking both potassium channels and gap junction coupling with intracellular loading of Cs^{+} and Ca^{2+}, we showed that only small currents could be activated by de- and hyperpolarization indicating that the major conductances in passive astrocytes in the striatum derive from potassium channels and gap junction coupling. When gap junctions are successfully blocked, the most prominent current detected should be potassium conductance. However, when potassium channels are blocked by intracellular loading of Cs^{+}, the membrane properties are distorted by potassium currents from surrounding cells. It is thus possible that the slow activating and deactivating components present in A1 and A2 astrocytes are derived from currents arising in connected cells. This is also supported by the finding that the prevalence of astrocytes expressing an A3 membrane current pattern increased during perfusion of 4-AP, and when gap junctions were blocked by Cbx or Ca^{2+}. However, the number of astrocytes exhibiting an A3 current pattern was not increased when gap junctions were blocked with octanol. The difference in membrane current pattern might be related to the potency of the uncoupling agents. But, since none of the drugs we used exclusively act on gap junction channels, the differences in membrane current pattern might be connected to different nonspecific effects of the different uncouplers (Marcet et al., 2004; Squecco et al., 2004; Swenson and Narahashi, 1980). However, the difference in membrane current pattern during impaired gap junction coupling might also imply that the time-dependent current components (A1, A2) derive from time-sensitive channels within the recorded cell. A recent study by Kimelberg and coworkers showed that outside-out membrane patches excised from cells that were previously whole-cell recorded showed a similar membrane current pattern, arguing that whole cell electrophysiological phenotype is an intrinsic property of the individual cell

(Schools et al., 2006). However, the phenotypes encountered in the hippocampus differ significantly from the striatum since the number of complex cells is high. Furthermore, our data are based on a subcategorization of passive astrocytes, which was not performed in the study by Kimelberg and co-workers (2006).

Blocking potassium channels with CsCl significantly reduced apparent capacitance, which suggests that gap junctions are affected under this recording condition. A previous study has shown that Cs^+ affects conductance of single connexin-43 channels (Valiunas et al., 1997). Since apparent capacitance was not significantly reduced in cells loaded with $CsMeSO_3$, but decreased when 0.5 mM $CaCl_2$ was added to the $CsMeSO_3$-solution, it is possible Cs^+-effects on the gap junction channel are modulated by $[Ca^{2+}]_i$.

Variable capacitance, which was detected in over 60% of the cells, has previously been shown in cultured neocortical and hippocampal stratum radiatum astrocytes (McKhann et al., 1997). The change in apparent capacitance suggests that gap junction conductance increases and decreases dynamically, which is also supported by our finding that capacitance was stable when gap junction coupling was blocked. Cell-to-cell connections can be affected by neuronal activity (Enkvist and McCarthy, 1994; Rouach et al., 2000), but are most likely not related to changes in intracellular calcium concentration since apparent capacitance also was unstable in BAPTA-filled cells (43%) (van den Pol et al., 1992). Since intracellular loading of Cs^+ significantly reduced the number of cells with variable capacitance, fluctuations in intracellular potassium concentration are thereby more likely candidates to underlie this dynamic coupling.

Astrocyte gap junction coupling

By loading one cell with Lucifer Yellow we were able to evaluate the extent of the astrocyte network. The number of cells stained after a 10 min incubation time was higher than that previously reported in studies of the hippocampus (Wallraff et al., 2004), and was also higher than the number observed in a previous study in rat striatum (Hamon et al., 2002). The gap junction permeability presented in our study could have been enhanced by a higher temperature and internal potassium concentration (Bukauskas and Weingart, 1993; Enkvist and McCarthy, 1994). Octanol and Cbx treatment significantly reduced the number of cells stained with Lucifer Yellow, indicating that gap junction permeability is related to the number of cells stained by Lucifer Yellow.

Blockade of gap junction coupling with octanol, Cbx or increased Ca^{2+} resulted in increased input resistance and reduced capacitance, which would be expected if gap junction channels are successfully closed (Blomstrand et al., 2004). The decrease in resting membrane potential detected after octanol and Cbx treatment could be due, at least in part, to closure of gap junctions. However, membrane potential was not affected when gap junctions were closed with high internal calcium. Furthermore, halothane, which potently closes gap junctions, does not affect resting potential (Hamon et al., 2002). Thus, it is not clear that all gap junction blockers produce this effect.

Since halothane was used as an anesthetic, gap junction coupling might be affected in these slices. However, halothane, a highly volatile compound, is fully removed from the preparation once the brain is detached and subjected to preincubation for 60 min before recordings are performed. In addition, the large number of cells loaded with Lucifer Yellow and the reduction in this number in slices perfused with octanol or carbanoxylone suggest that the gap junction coupling is functional at the onset of these recordings.

Morphological characterization of astrocytes post recording

The morphology of GFAP immunopositive passive astrocytes that were loaded with Lucifer Yellow varied extensively, and no specific attribute could be connected to a defined membrane current pattern. Since membrane current pattern was dependent on internal and external solutions, we do not expect the morphological properties to vary extensively between different subtypes of passive astrocytes. However, a previous study using transgenic mice with hGFAP promoter-controlled EGFP expression, suggested that hippocampal astrocyte subtypes display distinct morphological characteristics (Wallraff et al., 2004). However, due to the low number of complex astrocytes encountered in our study, we were unable to perform a morphological comparison between passive and complex astrocytes in the striatum.

Astrocyte function in the striatum

The basal ganglia are extensively involved in motor and cognitive functions (Graybiel et al., 1994), and the striatum, which is the biggest nucleus of the basal ganglia, plays a critical role in habit formation and motor sequencing (Balleine et al., 2007; Yin et al., 2005). Astrocytic uptake of glutamate and potassium from the synaptic cleft is crucial for neuronal functioning, and gap junction coupling might serve to augment the uptake capacity (Simard and Nedergaard, 2004; Waagepetersen et al., 2005). It is in this extent possible that the extensive gap junction coupling is required in order to fully support signal processing in the striatum.

The population of astrocytes appeared to be very homogenous in the striatum, with 94% expressing a passive membrane current pattern. However, this group could be sub-categorized, and the proportion of A1–A3 cells was dependent on the composition of the internal- and extracellular solutions. It is possible that the relative proportion of A1–A3 cells fluctuate in response to neuronal activity, but how this in turn might affect synaptic transmission in the striatum is beyond the scope of this study.

ACKNOWLEDGEMENTS

Margret I Davis is acknowledged for her helpful suggestions. This work was supported by the Division of Intramural Clinical and Basic Research, NIAAA, NIH, and The Swedish Society for Medical Research.

REFERENCES

Adermark L, Lovinger DM. Ethanol effects on electrophysiological properties of astrocytes in striatal brain slices. Neuropharmacology 2006;51:1099–1108. [PubMed: 16938316]

Adermark L, Olsson T, Hansson E. Ethanol acutely decreases astroglial gap junction permeability in primary cultures from defined brain regions. Neurochem Int 2004;45:971–978. [PubMed: 15337295]

Anderova M, Antonova T, Petrik D, Neprasova H, Chvatal A, Sykova E. Voltage-dependent potassium currents in hypertrophied rat astrocytes after a cortical stab wound. Glia 2004;48:311–326. [PubMed: 15390116]

Balleine BW, Delgado MR, Hikosaka O. The role of the dorsal striatum in reward and decision-making. J Neurosci 2007;27:8161–8165. [PubMed: 17670959]

Blomstrand F, Aberg ND, Eriksson PS, Hansson E, Ronnback L. Extent of intercellular calcium wave propagation is related to gap junction permeability and level of connexin-43 expression in astrocytes in primary cultures from four brain regions. Neuroscience 1999a;92:255–265. [PubMed: 10392848]

Blomstrand F, Khatibi S, Muyderman H, Hansson E, Olsson T, Ronnback L. 5-Hydroxytryptamine and glutamate modulate velocity and extent of intercellular calcium signalling in hippocampal astroglial cells in primary cultures. Neuroscience 1999b;88:1241–1253. [PubMed: 10336133]

Blomstrand F, Venance L, Siren AL, Ezan P, Hanse E, Glowinski J, Ehrenreich H, Giaume C. Endothelins regulate astrocyte gap junctions in rat hippocampal slices. Eur J Neurosci 2004;19:1005–1015. [PubMed: 15009148]

Bordey A, Sontheimer H. Electrophysiological properties of human astrocytic tumor cells In situ: enigma of spiking glial cells. J Neurophysiol 1998;79:2782–2793. [PubMed: 9582244]

Bukauskas FF, Weingart R. Temperature dependence of gap junction properties in neonatal rat heart cells. Pflugers Arch 1993;423:133–139. [PubMed: 7683787]

Chvatal A, Pastor A, Mauch M, Sykova E, Kettenmann H. Distinct populations of identified glial cells in the developing rat spinal cord slice: ion channel properties and cell morphology. Eur J Neurosci 1995;7:129–142. [PubMed: 7536092]

Cotrina ML, Lin JH, Alves-Rodrigues A, Liu S, Li J, Azmi-Ghadimi H, Kang J, Naus CC, Nedergaard M. Connexins regulate calcium signaling by controlling ATP release. Proc Natl Acad Sci U S A 1998;95:15735–15740. [PubMed: 9861039]

D'Ascenzo M, Fellin T, Terunuma M, Revilla-Sanchez R, Meaney DF, Auberson YP, Moss SJ, Haydon PG. mGluR5 stimulates gliotransmission in the nucleus accumbens. Proc Natl Acad Sci U S A 2007;104:1995–2000. [PubMed: 17259307]

Davis-Cox MI, Turner JN, Szarowski D, Shain W. Phorbol ester-stimulated stellation in primary cultures of astrocytes from different brain regions. Microsc Res Tech 1994;29:319–327. [PubMed: 7841503]

Dermietzel R, Hertberg EL, Kessler JA, Spray DC. Gap junctions between cultured astrocytes: immunocytochemical, molecular, and electrophysiological analysis. J Neurosci 1991;11:1421–1432. [PubMed: 1851221]

Dermietzel R, Spray DC. Gap junctions in the brain: where, what type, how many and why? Trends Neurosci 1993;16:186–192. [PubMed: 7685944]

Domaradzka-Pytel B, Ludkiewicz B, Jagalska-Majewska H, Morys J. Immunohistochemical study of microglial and astroglial cells during postnatal development of rat striatum. Folia Morphol (Warsz) 2000;58:315–323. [PubMed: 11000888]

Enkvist MO, McCarthy KD. Astroglial gap junction communication is increased by treatment with either glutamate or high K+ concentration. J Neurochem 1994;62:489–495. [PubMed: 7905024]

Freeman MR. Sculpting the nervous system: glial control of neuronal development. Curr Opin Neurobiol 2006;16:119–125. [PubMed: 16387489]

Giaume C, Venance L. Intercellular calcium signaling and gap junctional communication in astrocytes. Glia 1998;24:50–64. [PubMed: 9700489]

Graybiel AM, Aosaki T, Flaherty AW, Kimura M. The basal ganglia and adaptive motor control. Science 1994;265:1826–1831. [PubMed: 8091209]

Hamon, B.; Glowinski, J.; Giaume, C. Intracellular diffusional coupling between glial cells in the striatum. Totowa: Human Press; 2002. p. 99-112.

Isokawa M, McKhann GM 2nd. Electrophysiological and morphological characterization of dentate astrocytes in the hippocampus. J Neurobiol 2005;65:125–134. [PubMed: 16114022]

Marcet B, Becq F, Norez C, Delmas P, Verrier B. General anesthetic octanol and related compounds activate wild-type and delF508 cystic fibrosis chloride channels. Br J Pharmacol 2004;141:905–914. [PubMed: 14967738]

McKhann GM 2nd, D'Ambrosio R, Janigro D. Heterogeneity of astrocyte resting membrane potentials and intercellular coupling revealed by whole-cell and gramicidin-perforated patch recordings from cultured neocortical and hippocampal slice astrocytes. J Neurosci 1997;17:6850–6863. [PubMed: 9278520]

Nedergaard M, Ransom B, Goldman SA. New roles for astrocytes: redefining the functional architecture of the brain. Trends Neurosci 2003;26:523–530. [PubMed: 14522144]

Ransom B, Behar T, Nedergaard M. New roles for astrocytes (stars at last). Trends Neurosci 2003;26:520–522. [PubMed: 14522143]

Rouach N, Glowinski J, Giaume C. Activity-dependent neuronal control of gap-junctional communication in astrocytes. J Cell Biol 2000;149:1513–1526. [PubMed: 10871289]

Schipke CG, Kettenmann H. Astrocyte responses to neuronal activity. Glia 2004;47:226–232. [PubMed: 15252811]

Schools GP, Zhou M, Kimelberg HK. Development of gap junctions in hippocampal astrocytes: evidence that whole cell electrophysiological phenotype is an intrinsic property of the individual cell. J Neurophysiol 2006;96:1383–1392. [PubMed: 16775204]

Simard M, Nedergaard M. The neurobiology of glia in the context of water and ion homeostasis. Neuroscience 2004;129:877–896. [PubMed: 15561405]

Slezak M, Pfrieger FW. New roles for astrocytes: regulation of CNS synaptogenesis. Trends Neurosci 2003;26:531–535. [PubMed: 14522145]

Sontheimer H, Waxman SG, Ransom BR. Relationship between Na+ current expression and cell-cell coupling in astrocytes cultured from rat hippocampus. J Neurophysiol 1991;65:989–1002. [PubMed: 2051214]

Squecco R, Bencini C, Piperio C, Francini F. L-type Ca2+ channel and ryanodine receptor cross-talk in frog skeletal muscle. J Physiol 2004;555:137–152. [PubMed: 14660705]

Swenson RP, Narahashi T. Block of sodium conductance by n-octanol in crayfish giant axons. Biochim Biophys Acta 1980;603:228–236. [PubMed: 6257298]

Tepper JM, Abercrombie ED, Bolam JP. Basal ganglia macrocircuits. Prog Brain Res 2007;160:3–7. [PubMed: 17499105]

Valiunas V, Bukauskas FF, Weingart R. Conductances and selective permeability of connexin43 gap junction channels examined in neonatal rat heart cells. Circ Res 1997;80:708–719. [PubMed: 9130452]

van den Pol AN, Finkbeiner SM, Cornell-Bell AH. Calcium excitability and oscillations in suprachiasmatic nucleus neurons and glia in vitro. J Neurosci 1992;12:2648–2664. [PubMed: 1351936]

Venance L, Piomelli D, Glowinski J, Giaume C. Inhibition by anandamide of gap junctions and intercellular calcium signalling in striatal astrocytes. Nature 1995;376:590–594. [PubMed: 7637807]

Venance L, Premont J, Glowinski J, Giaume C. Gap junctional communication and pharmacological heterogeneity in astrocytes cultured from the rat striatum. J Physiol 1998;510(Pt 2):429–440. [PubMed: 9705994]

Waagepetersen HS, Qu H, Sonnewald U, Shimamoto K, Schousboe A. Role of glutamine and neuronal glutamate uptake in glutamate homeostasis and synthesis during vesicular release in cultured glutamatergic neurons. Neurochem Int 2005;47:92–102. [PubMed: 15921825]

Wallraff A, Kohling R, Heinemann U, Theis M, Willecke K, Steinhauser C. The impact of astrocytic gap junctional coupling on potassium buffering in the hippocampus. J Neurosci 2006;26:5438–5447. [PubMed: 16707796]

Wallraff A, Odermatt B, Willecke K, Steinhauser C. Distinct types of astroglial cells in the hippocampus differ in gap junction coupling. Glia 2004;48:36–43. [PubMed: 15326613]

Yin HH, Ostlund SB, Knowlton BJ, Balleine BW. The role of the dorsomedial striatum in instrumental conditioning. Eur J Neurosci 2005;22:513–523. [PubMed: 16045504]

Zhou M, Schools GP, Kimelberg HK. Development of GLAST(+) astrocytes and NG2(+) glia in rat hippocampus CA1: mature astrocytes are electrophysiologically passive. J Neurophysiol 2006;95:134–143. [PubMed: 16093329]

Abbreviations used in the text

GFAP, Glial fibrillary acidic protein; Cbx, Carbenoxolone; 4-AP, 4-aminopyridine..

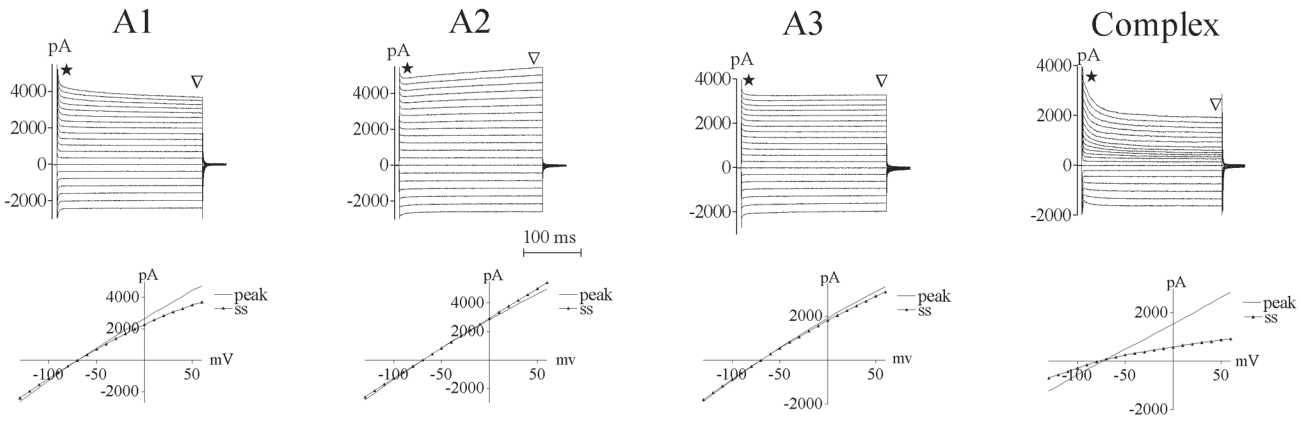

Figure 1.

Astrocyte subtypes were categorized based on physiological criteria's. All passive cells displayed large voltage independent currents. (a) Cells with an A1 current pattern (56%) also had a slowly decaying current component, while A2 astrocytes (19%) displayed a slowly activating component (b). (c) A3 astrocytes (20%) only showed time- and voltage independent conductance. (d) Complex astrocytes expressed a combination of time- and voltage-activated conductances. To activate the currents, cells were held at −70 mV and 10 mV hyperpolarizing and depolarizing voltage steps of 250 ms duration were applied in both hyperpolarizing and depolarizing direction (+ 60 to − 130 (+ 100 to − 90 for the complex cell)). Current/voltage relationship was measured for both peak and steady-state (ss) components of current.

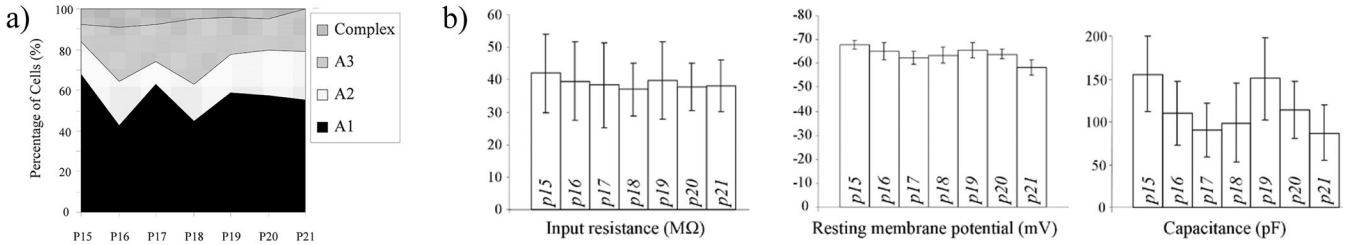

Figure 2.

Developmental properties of p15 to p21 astrocytes. a) The proportion of electrophysiologically-defined astrocyte subtypes did not vary across the age range evaluated here. b) Resting membrane potential in cells from P21 slices were more positive in comparison to cells at earlier developmental time points (P15 $p < 0.001$; P16 $p < 0.05$; P19 $p < 0.05$), but input resistance and apparent capacitance did not differ significantly within this age span. Each group represents data from 22 to 40 patch clamped astrocytes from at least 3 different animals. The total number of cells analyzed was 217. Data are presented as mean values with 95% CI and statistical comparisons between groups of cells were performed by one-way ANOVA with Tukey's Multiple Comparison Test, or Fisher's exact test.

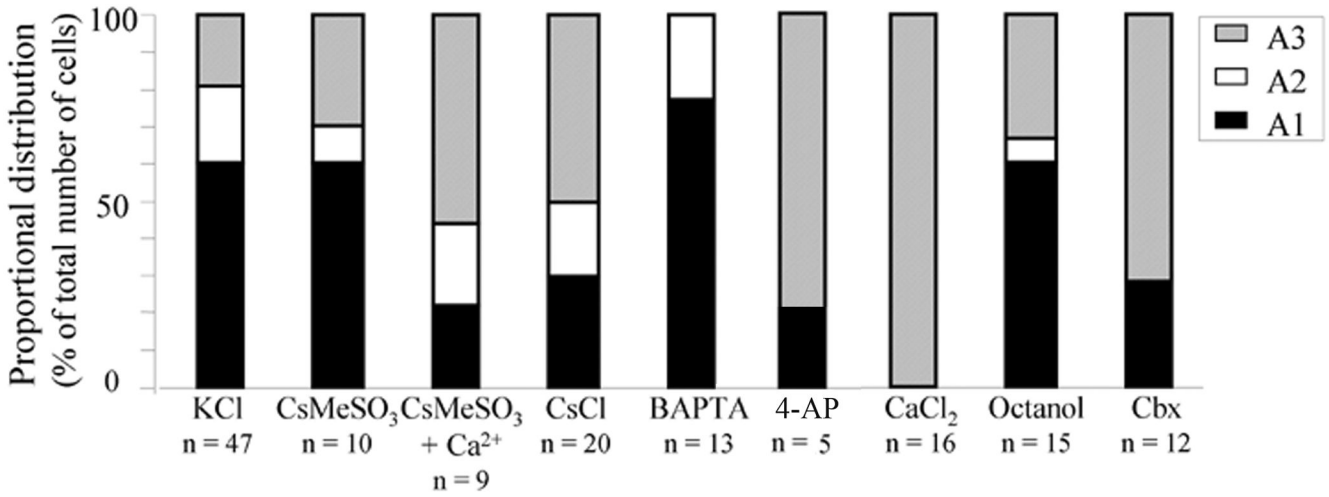

Figure 3.

The relative proportion of different striatal subtypes is modulated by the composition of the internal solution and gap junction coupling. The number of A1 expressing astrocytes was significantly reduced in astrocytes patch clamped with an internal solution containing CsCl or increased $[Ca^{2+}]_i$. Blocking gap junction coupling by Cbx (100 μM) or intracellular loading with $CaCl_2$ (2 mM), increased the number of cells with an A3 membrane current pattern, while no A3-subtypes were detected when intracellular calcium was chelated with BAPTA. Graph showing proportional representation of the different subtypes of passive astrocytes. Each group is based on recordings from at least 3 different animals.

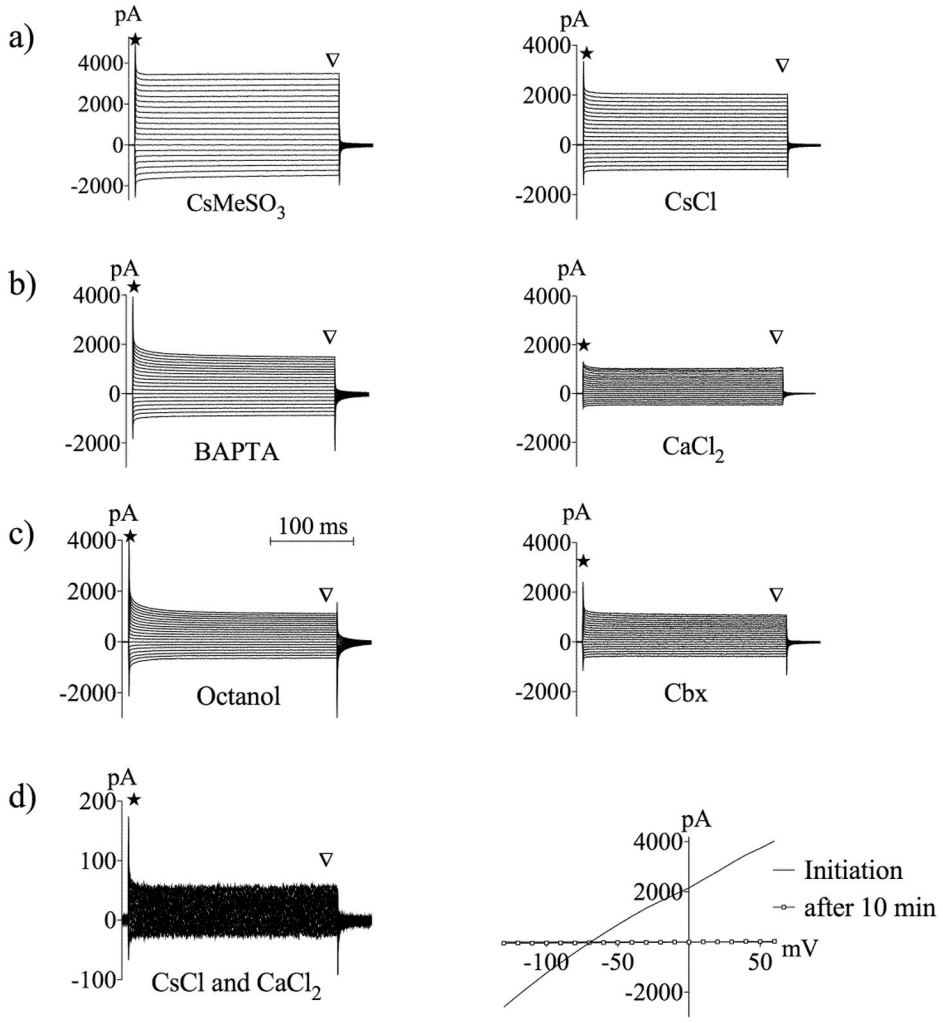

Figure 4.

Representative traces showing membrane current pattern during reduction of specific conductances. a) Potassium channels were blocked by intracellular Cs^+-loading. b) Intracellular calcium was chelated by 10 mM BAPTA or increased by intracellular loading with 2 mM $CaCl_2$. In the presence of elevated intracellular calcium, transients at the start and end of current pulses are diminished, indicative of decreased apparent capacitance (star), and current amplitude during voltage steps is also decreased, indicative of decreased conductance. c) Recordings during extracellular treatment with 1 mM octanol or extracellular application of 100 μM Cbx. Note the diminished transients and current, indicating decreases in apparent capacitance and conductance, respectively. d) Recordings in the combined presence of Cs^+ and elevated intracellular Ca^{2+}. Passive conductances are greatly diminished under this condition. Note the expanded current scale. Right hand figure shows I/V relationship at steady state (arrowhead) immediately after establishing the whole cell recording and 15 min later when the CsCl and high $[Ca^{2+}]_i$-containing internal solution has diffused into the cell. Currents were activated in response to increasing hyper- and depolarizing potentials ranging from −130 to 60 mV, in 10 mV increments.

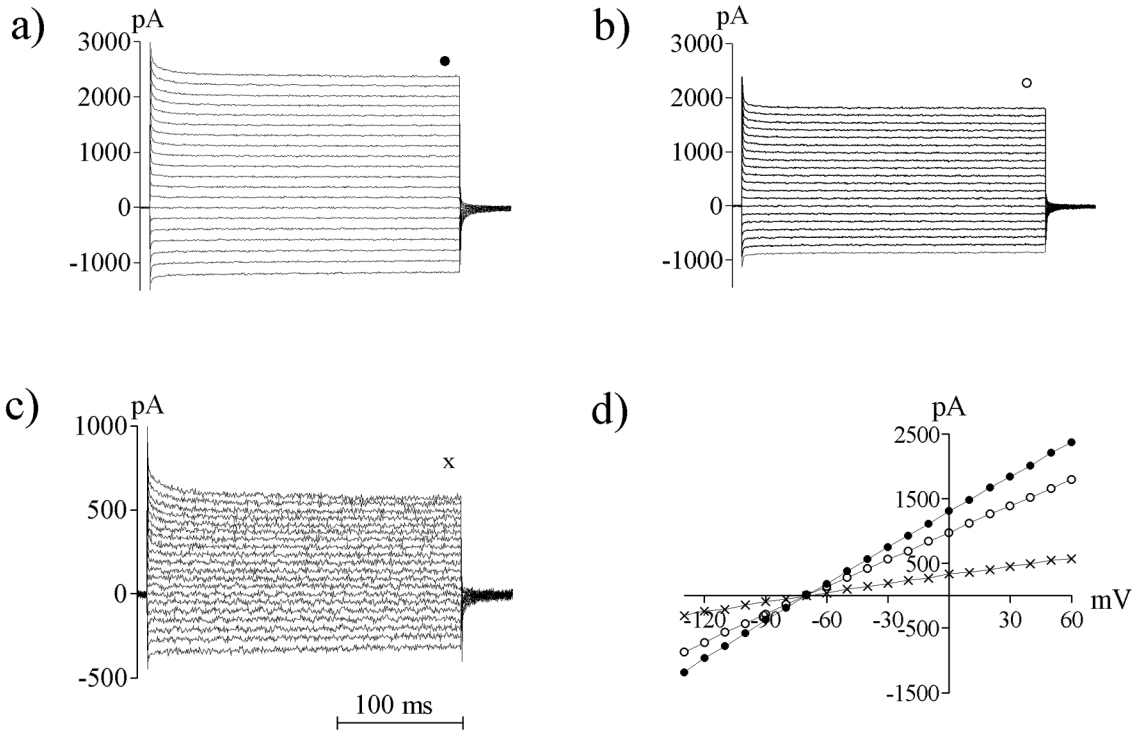

Figure 5.

Striatal astrocytes displayed 4-AP-sensitive outward K^+ currents. The 4-AP sensitive current (c), was obtained by subtracting the current observed during 4-AP exposure (4 mM) (b) from the baseline conductance (a). d) Graph show I/V relationships for baseline current (●), 4-AP insensitive current (○), and 4-AP sensitive current (X) from one representative experiment. A stable I/V relationship was required before slices were treated with 4-AP.

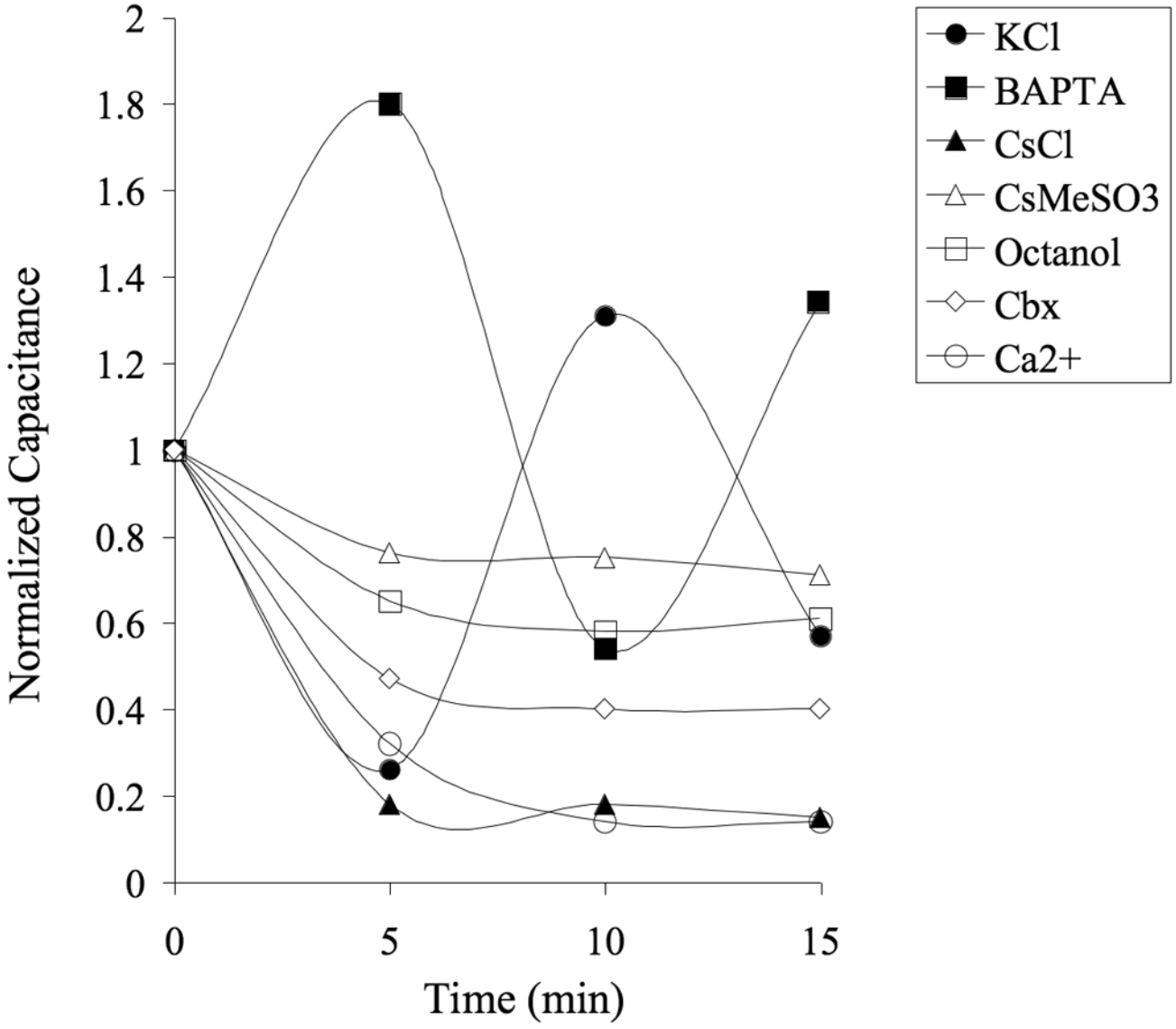

Figure 6.

Capacitance fluctuates over time in patch clamped astrocytes. Measured capacitance stabilized within 5 min after established whole cell configuration in 90% of the cells loaded with Cs^+-based internal solution, but varied extensively (> 30 pF) in 62% of the astrocytes loaded with a KCl-based internal solution. None of the cells treated with gap junction blockers exhibited an unstable capacitance. Graph shows normalized capacitance in representative astrocytes.

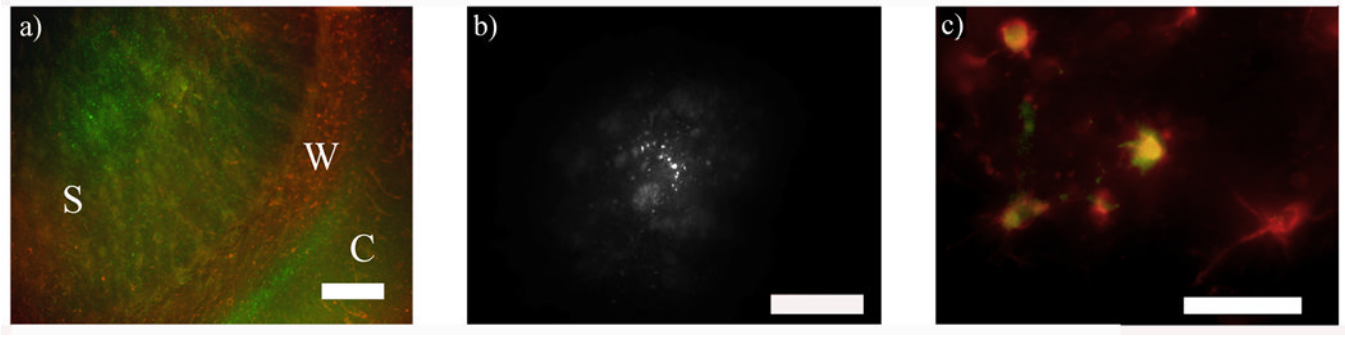

Figure 7.
Dye coupling and immunohistochemistry. a) Intracellular staining of Lucifer Yellow revealed an extensive astrocytic network in the striatum that also included cells in the cortex. To be able to show the whole network the amplification is low and therefore Lucifer Yellow stained astrocytes appear as very small green puncta. S = striatum, W = white matter, C = cortex. (GFAP, red, Lucifer Yellow, green). b) The number of cells loaded with Lucifer Yellow was significantly reduced in slices perfused with octanol (1 mM). Note the different scale in comparison to a. c) Cells loaded with Lucifer Yellow were immunopositive for GFAP, showing that patch clamped cells are astrocytes. GFAP, red; Lucifer Yellow, green. Scale bar is 200 μm in a, 100 μm in b and 20 μm in c.

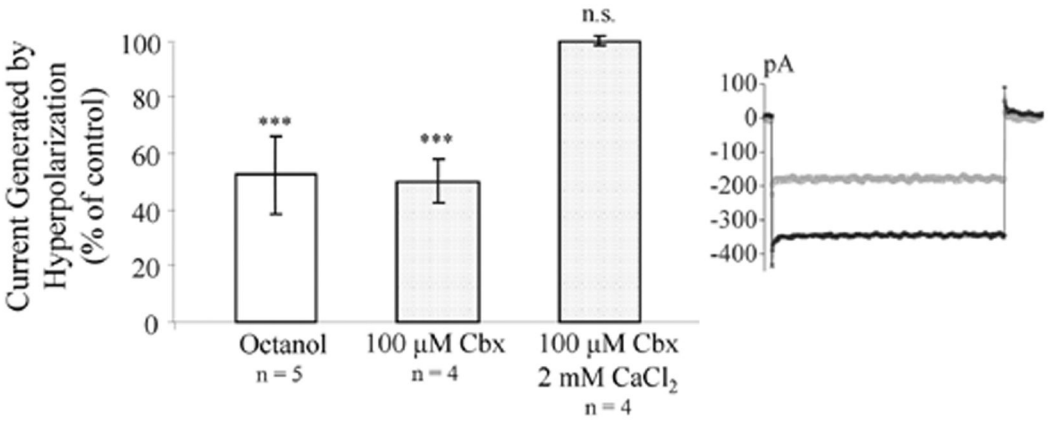

Figure 8.

Changes in gap junction coupling alters astrocyte electrophysiological responses. Extracellular application of 1 mM octanol or 100 µM Cbx significantly reduced the current response to a hyperpolarizing pulse (−20 mV) in KCl-loaded astrocytes. Cbx did not reduce activated current in astrocytes were gap junction coupling was blocked by high $[Ca^{2+}]_i$. Patch clamped cells were held at −70 mV and a stable baseline was required before extracellular application of gap junction blockers. Example traces show baseline current (black) and after Cbx treatment (gray). *** $p < 0.001$.

Table I

Intrinsic properties of astrocytes with specific membrane current patterns

	A1 n = 122	A2 n = 41	A3 n = 43	Complex n = 11
IR (MΩ)	32 ± 4.3	32 ± 7.6	36 ± 5.8	133 ± 28 [a]
Vm (mV)	− 62 ± 1.5	− 65 ± 2.2	− 61 ± 3.2	− 71 ± 3.2 [b]
C (pF)	121 ± 21	149 ± 40	86 ± 28 [c]	51 ± 22 [c]

[a] $p < 0.001$ in comparison to passive astrocytes (A1 – A3).

[b] $p < 0.01$ when compared to A1 and A3 astrocytes.

[c] $p < 0.05$ when compared to A2.

Table II

Intrinsic properties of passive astrocytes under different treatment conditions [#]

	KCl n = 47	$CsMeSO_3$ n = 18	$CsMeSO_3$ + $CaCl_2$ n = 9	CsCl n = 20	BAPTA n = 10	CaCl n = 16	Octanol n = 14	Cbx n = 12	Cs^+ + Ca^{2+} n = 7
IR (MΩ)	41 ± 3.9	51 ± 6.4	44 ± 9.2	61 ± 8.3	48 ± 12	108 ± 17 ***	119 ± 23 ***	98 ± 19 ***	1530 ± 220 ***
Vm (mV)	−64 ± 2.1	−54 ± 4.1	−59 ± 12	−61 ± 5.0	−67 ± 8.8	−58 ± 7.9	−42 ± 9.0 **	−51 ± 6.8 *	−19 ± 10 ***
C (pF)	105 ± 28	95 ± 50	8.3 ± 2.4 ***	11 ± 5.0 ***	123 ± 59	12 ± 5.5 **	15 ± 2.7 **	16 ± 6.2 *	3.3 ± 1.4 ***

[#] 15 min after initiating whole-cell recording. *p* values show the level of significance in comparison to KCl filled cells.

* $p < 0.05$

** $p < 0.01$

*** $p < 0.001$